



# Superior activity of $\text{MnO}_x\text{-CeO}_2/\text{TiO}_2$ catalyst for catalytic oxidation of elemental mercury at low flue gas temperatures

Hailong Li<sup>a,b</sup>, Chang-Yu Wu<sup>b,\*</sup>, Ying Li<sup>c</sup>, Junying Zhang<sup>a</sup>

<sup>a</sup> State Key Laboratory of Coal Combustion, Huazhong University of Science and Technology, Wuhan, Hubei 430074, China

<sup>b</sup> Department of Environmental Engineering Sciences, University of Florida, Gainesville, FL 32611, United States

<sup>c</sup> Department of Mechanical Engineering, University of Wisconsin-Milwaukee, Milwaukee, WI 53211, United States

## ARTICLE INFO

### Article history:

Received 21 July 2011

Received in revised form

25 September 2011

Accepted 11 October 2011

Available online 18 October 2011

### Keywords:

Mercury

Manganese oxide

Cerium oxide

Catalyst

Coal combustion

## ABSTRACT

$\text{TiO}_2$  supported Mn-Ce mixed oxides (Mn-Ce/Ti) synthesized by an ultrasound-assisted impregnation method were employed to oxidize elemental mercury ( $\text{Hg}^0$ ) at low temperatures in simulated low-rank (sub-bituminous and lignite) coal combustion flue gas and corresponding selective catalytic reduction (SCR) flue gas. The catalysts were characterized by BET surface area analysis, X-ray diffraction (XRD) measurement and X-ray photoelectron spectroscopy (XPS) analysis. The combination of  $\text{MnO}_x$  and  $\text{CeO}_2$  resulted in significant synergy for  $\text{Hg}^0$  oxidation. The Mn-Ce/Ti catalyst was highly active for  $\text{Hg}^0$  oxidation at low temperatures (150–250 °C) under both simulated flue gas and SCR flue gas. The dominance of  $\text{Mn}^{4+}$  and the presence of  $\text{Ce}^{3+}$  on the Mn-Ce/Ti catalyst were responsible for its excellent catalytic performance.  $\text{Hg}^0$  oxidation on the Mn-Ce/Ti catalyst likely followed the Langmuir–Hinshelwood mechanism, where reactive species on catalyst surface react with adjacently adsorbed  $\text{Hg}^0$  to form  $\text{Hg}^{2+}$ .  $\text{NH}_3$  consumed the surface oxygen and limited the adsorption of  $\text{Hg}^0$ , hence inhibiting  $\text{Hg}^0$  oxidation over Mn-Ce/Ti catalyst. However, once  $\text{NH}_3$  was cut off, the inhibited mercury oxidation activity could be completely recovered in the presence of  $\text{O}_2$ . This study revealed the possibility of simultaneously oxidizing  $\text{Hg}^0$  and reducing  $\text{NO}_x$  at low flue gas temperatures. Such knowledge is of fundamental importance in developing effective and economical mercury and  $\text{NO}_x$  control technologies for coal-fired power plants.

© 2011 Elsevier B.V. All rights reserved.

## 1. Introduction

Emission of mercury (Hg) from anthropogenic sources into the atmosphere has become a major environmental issue that attracts considerable public attention because of the extreme toxicity, persistence, and bioaccumulation of methyl mercury transformed from emitted mercury [1]. Coal combustion has been targeted as a major source of anthropogenic mercury emissions in the United States. It is estimated that about one-third of the known anthropogenic mercury emissions in the United States is from coal combustion [2,3]. By April 2010 more than 20 U.S. states had proposed or adopted mercury emission regulations which were more stringent than the Clean Air Mercury Rule (CAMR) to regulate mercury emissions from coal-fired power plants [4]. The U.S. Environmental Protection Agency (EPA) has also proposed federal mercury and air toxics standards to limit mercury emission from power plants [5]. To meet the demands of these mercury regulations, effective control technologies are urgently needed.

Activated carbon injection (ACI) is the maximum achievable control technology (MACT) for mercury emission control from coal-fired power plants. Other technologies such as catalytic oxidation plus wet flue gas desulfurization (WFGD) have also been widely investigated. The efficacy of mercury control methods depends largely on the form and species of mercury [6]. Mercury in coal combustion derived flue gas is present in three forms i.e., elemental mercury ( $\text{Hg}^0$ ), oxidized mercury ( $\text{Hg}^{2+}$ ) and particulate-bound mercury ( $\text{Hg}^p$ ) [7].  $\text{Hg}^p$  can be captured by particulate matter (PM) control devices such as electrostatic precipitators (ESP) and fabric filters (FF). Water-soluble  $\text{Hg}^{2+}$  is readily captured in WFGD system [7], and it can also be adsorbed on fly ash and subsequently collected along with fly ash in PM control devices. In contrast,  $\text{Hg}^0$  vapor is most likely to escape from existing air pollution control devices (APCDs) because it is highly volatile and nearly insoluble in water [8]. As such,  $\text{Hg}^0$  is the dominant mercury species emitted to the atmosphere. For example,  $\text{Hg}^0$  accounts for 66–94% of total mercury emitted from coal-fired power plants in China [9], and 67% for coal-fired power plants in Texas [10]. Consequently, catalysts capable of significant conversion (>80%) of  $\text{Hg}^0$  to  $\text{Hg}^{2+}$  would have tremendous value [11] because  $\text{Hg}^{2+}$  can be removed simultaneously with PM and acid gases in ESP/FF and WFGD, respectively.

\* Corresponding author. Tel.: +1 352 392 0845; fax: +1 352 392 3076.

E-mail address: [cwu@ufl.edu](mailto:cwu@ufl.edu) (C.-Y. Wu).

Selective catalytic reduction (SCR) catalyst has been successfully used in coal-fired power plants to control NO<sub>x</sub> emissions for decades. In addition to NO<sub>x</sub> control, SCR catalysts exhibit the co-benefit of promoting mercury oxidation in coal-fired power plants [12–17]. This co-benefit from SCR makes the cost of mercury control more economical than the ACI method. The required operating temperature of conventional vanadia based SCR catalysts is typically at 300–400 °C. Accordingly, it is necessary to locate the SCR unit upstream of the ESP/FF and WFGD immediately after the steam generator in order to avoid the cost for reheating the flue gas. However, this accelerates the catalyst deactivation through exposure to high concentrations of PM [18]. To avoid the deactivation by PM, it is therefore desirable to develop a SCR catalyst with high activity at low temperatures (100–250 °C), which would allow the SCR reactor to be located downstream of the PM control devices where the flue gas is relatively clean. Smirniotis and co-workers [19,20] studied the low temperature SCR performances of several metal oxides supported on TiO<sub>2</sub>, and found that MnO<sub>x</sub> supported on Hombikat TiO<sub>2</sub> exhibited the best performance with 100% NO conversion at temperatures as low as 120 °C. MnO<sub>x</sub>/TiO<sub>2</sub> (Mn/Ti) catalysts have also been proposed as economical low temperature SCR catalysts for controlling NO<sub>x</sub> emission in many other research studies [21–23]. Meanwhile, MnO<sub>x</sub> based catalysts [23–25] have been studied as potential catalysts for Hg<sup>0</sup> oxidation, too. In other words, MnO<sub>x</sub> based SCR catalyst can also serve as a catalyst for Hg<sup>0</sup> oxidation, as reported by Ji et al. [23] that MnO<sub>x</sub> supported on titania was effective for both Hg<sup>0</sup> oxidation and low temperature SCR of NO<sub>x</sub>. Recently, CeO<sub>2</sub> has also been extensively studied for selective catalytic reduction of NO<sub>x</sub> due to its large oxygen storage capacity and unique redox couple Ce<sup>3+</sup>/Ce<sup>4+</sup> with the ability to shift between CeO<sub>2</sub> and Ce<sub>2</sub>O<sub>3</sub> under oxidizing and reducing conditions, respectively [26]. Mn–Ce mixed-oxide was synthesized and found to be an excellent low-temperature SCR catalyst [27–29]. For industrial applications, active catalysts are usually supported by carriers such as TiO<sub>2</sub>, which provides high surface area, high thermal stability, strong mechanical strength and high sulfur resistance. Therefore, TiO<sub>2</sub> supported Mn–Ce mixed oxide (Mn–Ce/Ti) has been recently developed as a SCR catalyst with extraordinarily high activity for NO<sub>x</sub> removal [30,31]. However, no research on Hg<sup>0</sup> oxidation over low temperature Mn–Ce/Ti catalysts has been reported to date.

In this work, Mn–Ce/Ti catalysts prepared by an ultrasound-assisted impregnation method were employed to oxidize Hg<sup>0</sup> to Hg<sup>2+</sup> in simulated flue gas from combustion of low-rank coals (sub-bituminous and lignite) and corresponding SCR flue gas. The mechanism involved in Hg<sup>0</sup> oxidation was examined. Effects of catalyst composition and flue gas condition were investigated as well.

## 2. Experimental

### 2.1. Preparation of catalysts

The Mn/Ti, CeO<sub>2</sub>/TiO<sub>2</sub> (Ce/Ti) and Mn–Ce/Ti catalysts were synthesized using manganese nitrate (Tetrahydrate, for analysis, Acros Organics) and/or cerium nitrate (Hexahydrate 99.5%, Acros Organics) aqueous solution and TiO<sub>2</sub> nano-particles (P25, Evonik) by an impregnation method enhanced by ultrasound [32]. After stirring for 30 min, the mixture was exposed to an ultrasonic bath for 2 h, dried at 110 °C overnight and calcined at 500 °C in static air for 4 h. Powder form catalysts were obtained by grinding the composite and sieving through 100 meshes (150 μm). The mass ratio of CeO<sub>2</sub>/TiO<sub>2</sub> in the Ce/Ti catalysts was 1:1, which was found in our preliminary study to be close to the optimal ratio of Ce/Ti catalysts for Hg<sup>0</sup> oxidation [33]. For the Mn–Ce/Ti catalyst, the mass ratio of

MnO<sub>2</sub>/CeO<sub>2</sub>/TiO<sub>2</sub> was 0.18:0.82:1. The corresponding molar ratio of Mn/(Ce + Mn) was 0.3, which was the optimal ratio of MnO<sub>x</sub>–CeO<sub>2</sub> catalyst for selective catalytic reduction of NO<sub>x</sub> [29]. The content of manganese oxides (calculated as MnO<sub>2</sub>) in the Mn/Ti catalysts was the same as that in the Mn–Ce/Ti catalyst, and it was also close to the optimal MnO<sub>2</sub>/TiO<sub>2</sub> mass ratio of Mn/Ti SCR catalyst synthesized using P25 TiO<sub>2</sub> [18].

### 2.2. Characterization of catalysts

Brunauer–Emmett–Teller (BET) surface area analysis by N<sub>2</sub> adsorption was performed using a Quantachrome NOVA 1200 gas sorption analyzer (Boynton Beach, FL). Prior to BET measurements, every sample was oven dried at 110 °C overnight, and then degassed at 180 °C for 12 h under vacuum. X-ray diffraction (XRD) measurement was carried out in a Philips APD 3720 diffractometer using Cu Kα radiation (λ = 0.1542 nm) in the range of 20–60° (2θ) with a step size of 0.02°. X-ray photoelectron spectroscopy (XPS) analysis was carried out in a Perkin–Elmer PHI 5100 ESCA system operating at 8 × 10<sup>−10</sup> Torr with an Al Kα X-ray source (hν = 1486.6 eV) and pass energy of 35.75 eV. All oven-dried samples were outgassed in a vacuum oven for 12 h before XPS analysis. The observed spectra were corrected with the C 1s binding energy (BE) value of 284.6 eV. The AugerScan Demo program was employed to fit the XPS spectra.

### 2.3. Catalytic activity measurement

The catalytic activities were evaluated using a bench-scale experimental system, which is similar to that used in our previous study [34] and is shown in Fig. 1. In each test, catalyst was loaded in a Pyrex reactor, which was placed in the temperature controlled tubular furnace to control the reaction temperature. All individual flue gas components were from cylinder gases and were precisely controlled by mass flow controllers, with a total flow rate of 1 L min<sup>−1</sup>. Water vapor was generated using a heated water bubbler. A Dynacal Hg<sup>0</sup> permeation device (VICI Metronics) was used to provide a constant feed of Hg<sup>0</sup> concentration (~75 μg m<sup>−3</sup>). The relatively high Hg<sup>0</sup> concentration was employed to reduce the experimental errors caused by the sensitivity of the mercury analyzer and to allow experiments to be completed in a reasonable time scale. An RA-915+ mercury analyzer (OhioLumex, essentially a portable Zeeman-modulated cold vapor atomic absorption apparatus) was employed to measure Hg<sup>0</sup> concentrations at both the inlet and outlet of the reactor. It was verified that interferences on Hg<sup>0</sup> measurement by an empty reactor and flue gas components such as water vapor were negligible. Even so, before proceeding to the mercury analyzer, acid gases and water vapor were removed from the sample flow at the end of the Hg speciation conversion system and the condenser, respectively.

At the beginning of each test, the gas stream bypassed the reactor and the inlet gas was sampled to ensure a stable Hg<sup>0</sup> feed concentration (Hg<sup>0</sup><sub>in</sub>). Then, gas flow passed through the catalyst was taken from the exit of the reactor to get the outlet Hg<sup>0</sup> concentration (Hg<sup>0</sup><sub>out</sub>). Hg<sup>0</sup><sub>out</sub> was recorded after the process had reached equilibrium, which was defined as having fluctuation of Hg<sup>0</sup> concentration less than 5% for more than 2 h. At the end of each test, the mercury analyzer was switched to the reactor inlet to verify the Hg<sup>0</sup><sub>in</sub>. The loss of Hg<sup>0</sup> over the catalysts could be due to conversion to an oxidized form that is adsorbed, or the adsorption of Hg<sup>0</sup>, or a combination of both [35]. However, it is generally agreed that most of the decrease in Hg<sup>0</sup> concentration across catalysts is attributed to Hg<sup>0</sup> oxidation [36,37]. Therefore, for our reporting of the results, the difference between the inlet and outlet Hg<sup>0</sup> was considered to be the oxidized mercury, and the definition of Hg<sup>0</sup> oxidation

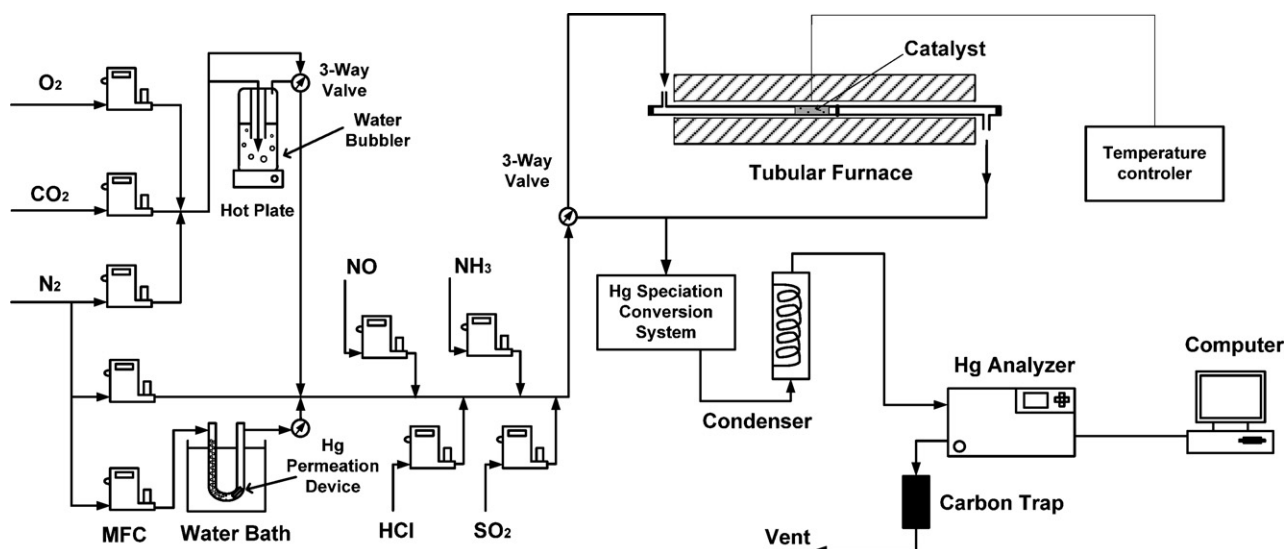


Fig. 1. Schematic diagram of the experimental system.

efficiency ( $E_{\text{oxi}}$ ) is as Eq. (1), which is the same as those over other catalysts [36–38].

$$E_{\text{oxi}}(\%) = \frac{\Delta \text{Hg}^0}{\text{Hg}_{\text{in}}^0} = \frac{\text{Hg}_{\text{in}}^0 - \text{Hg}_{\text{out}}^0}{\text{Hg}_{\text{in}}^0} \times 100\% \quad (1)$$

### 3. Results

#### 3.1. Characterization of catalysts

The BET surface areas of the Mn/Ti, Ce/Ti and Mn-Ce/Ti catalysts are listed in Table 1. Surface areas of all these catalysts were about  $55 \text{ m}^2 \text{ g}^{-1}$ , which is close to the surface areas of Mn/Ti and Mn-Ce/Ti catalysts reported in another literature [30]. Mn/Ti catalyst showed the lowest surface area of  $53.1 \text{ m}^2 \text{ g}^{-1}$ , while Ce/Ti catalyst exhibited the highest surface area of  $61.1 \text{ m}^2 \text{ g}^{-1}$ , but they are not very different.

The XRD patterns of Mn/Ti, Ce/Ti and Mn-Ce/Ti catalysts are shown in Fig. 2. Crystalline phases were identified by comparison with ICDD files. For the Mn/Ti catalyst, both anatase  $\text{TiO}_2$  and rutile  $\text{TiO}_2$  were detected, with anatase being the dominating phase. Only few weak peaks from crystalline manganese oxide were observed, indicating that most manganese was well incorporated into the matrix of  $\text{TiO}_2$  and/or the manganese oxide was highly dispersed on the  $\text{TiO}_2$  support, i.e. existing in an amorphous or poorly crystalline state [21]. For the Ce/Ti catalyst, anatase  $\text{TiO}_2$  was also detected to be the predominant  $\text{TiO}_2$  form, and cubic  $\text{CeO}_2$  phase was observed. This is in line with other study that cubic  $\text{CeO}_2$  was observed when the mass ratio of  $\text{CeO}_2/\text{TiO}_2$  exceeded 0.2 in Ce/Ti catalysts prepared by an impregnation method [39]. Compared to the XRD patterns of Mn/Ti and Ce/Ti catalysts,  $\text{TiO}_2$  and  $\text{CeO}_2$  peaks on the XRD pattern of Mn-Ce/Ti catalyst became much weaker, and the peaks attributed to crystalline manganese oxides disappeared.

**Table 1**  
BET surface area and surface atomic concentration of the studied catalysts.

Catalysts	BET surface area ( $\text{m}^2 \text{ g}^{-1}$ )	Surface atomic concentration (%)			
		Mn	Ce	Ti	O
Mn/Ti	53.1	2.4	0.0	19.4	78.2
Ce/Ti	61.1	0.0	9.7	8.4	81.9
Mn-Ce/Ti	55.7	3.3	4.3	6.1	86.3

This indicates that there were intense interactions between these three metal oxides. The interactions probably include the incorporation of  $\text{Ti}^{4+}$  into  $\text{CeO}_2$  lattice [40], the incorporation of  $\text{Mn}^{4+}$  into  $\text{TiO}_2$  lattice [21,41] and the incorporation of Mn atoms into  $\text{CeO}_2$  lattice [27]. These interactions resulted in more amorphous metal oxides on the Mn-Ce/Ti catalyst, which are more active than crystalline phase for catalytic process.

The XPS spectra of Mn 2p for Mn/Ti and Mn-Ce/Ti catalysts are shown in Fig. 3. Two primary peaks due to Mn 2p<sub>3/2</sub> and Mn 2p<sub>1/2</sub> were observed from 630 to 660 eV. The Mn 2p<sub>3/2</sub> peak consists of two sub-peaks:  $\text{Mn}^{4+}$  peak at about 642.7 eV and  $\text{Mn}^{3+}$  peak at about 641.2 eV [25,42,43]. When  $\text{CeO}_2$  was added into the Mn/Ti catalyst to form Mn-Ce/Ti catalyst, the ratio of  $\text{Mn}^{4+}/\text{Mn}^{3+}$  increased significantly, which was favorable for  $\text{Hg}^0$  oxidation [24].

The XPS spectra of Ce 3d for Ce/Ti and Mn-Ce/Ti catalysts are shown in Fig. 4(a) and (b). The peaks labeled  $u$  are due to 3d<sub>3/2</sub> spin-orbit states, and those labeled  $v$  are the corresponding 3d<sub>5/2</sub> states [26]. The  $u/v$ ,  $u_2/v_2$  and  $u_3/v_3$  doublets represent the 3d<sup>10</sup>4f<sup>0</sup> state of  $\text{Ce}^{4+}$ , while the doublet labeled  $u_1/v_1$  represents the 3d<sup>10</sup>4f<sup>1</sup> initial electronic state corresponding to  $\text{Ce}^{3+}$  [44,45]. In both Ce/Ti and Mn-Ce/Ti catalysts, the peaks attributed to  $\text{Ce}^{4+}$  were

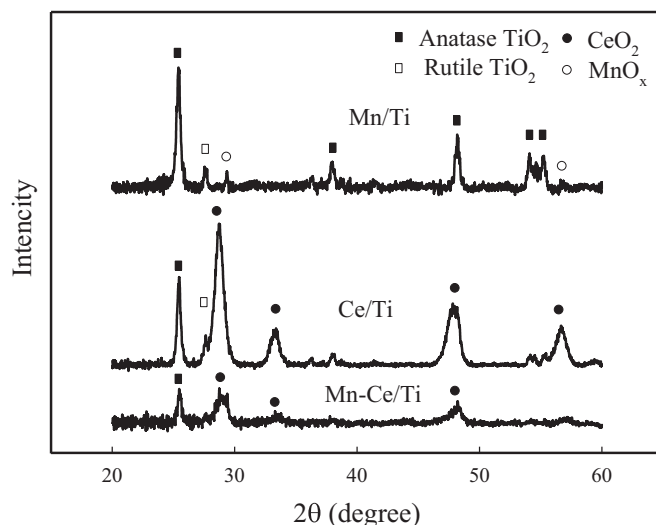


Fig. 2. XRD profiles of Mn/Ti, Ce/Ti and Mn-Ce/Ti catalysts.

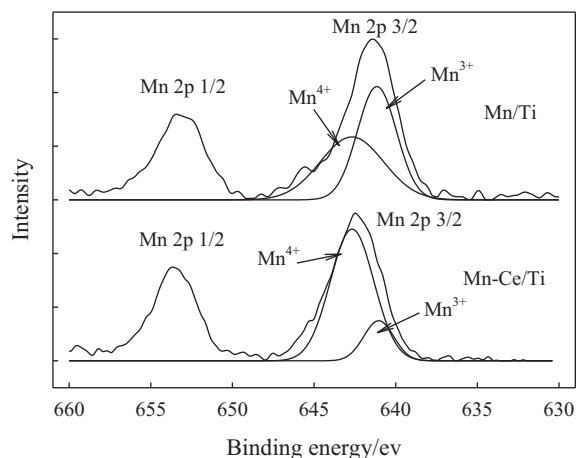


Fig. 3. Mn 2p patterns of Mn/Ti and Mn-Ce/Ti catalysts.

predominant, while as shown in Fig. 4(b) the small peak of  $\nu 1$  evidenced the presence of  $\text{Ce}^{3+}$  over Ce/Ti and Mn-Ce/Ti catalysts. The presence of the  $\text{Ce}^{3+}$  could create charge imbalance, vacancies and unsaturated chemical bonds on the catalyst surface [46], which lead to the increase of surface chemisorbed oxygen [47]. When  $\text{MnO}_x$  and  $\text{CeO}_2$  were combined together the ratio of  $\text{Ce}^{3+}/\text{Ce}^{4+}$  also increased that would result in more surface oxygen for  $\text{Hg}^0$  oxidation.

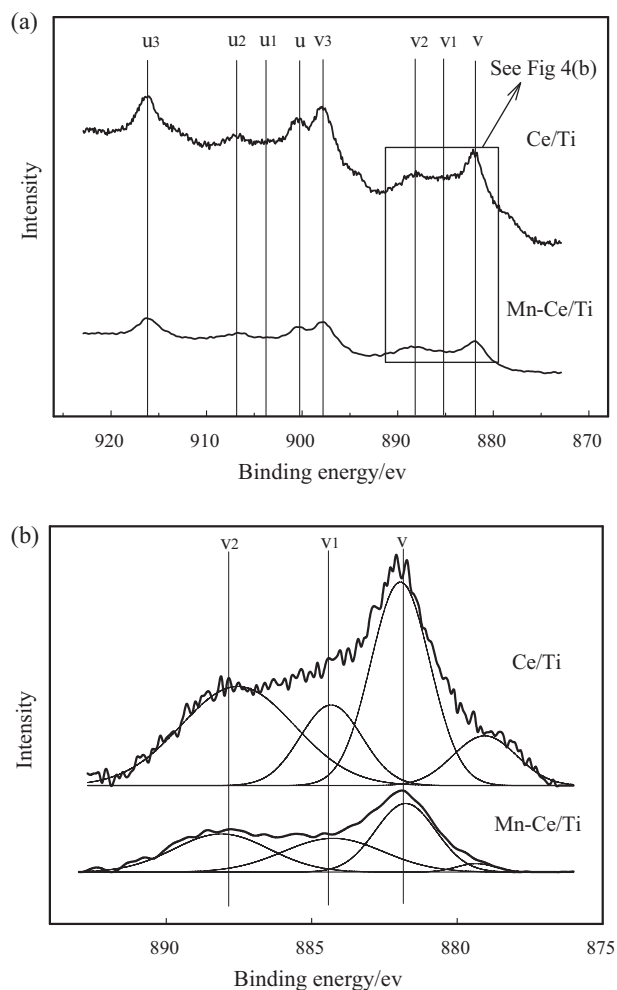


Fig. 4. (a) Ce 3d patterns of Ce/Ti and Mn-Ce/Ti catalysts; (b) Magnification of the marked XPS spectra.

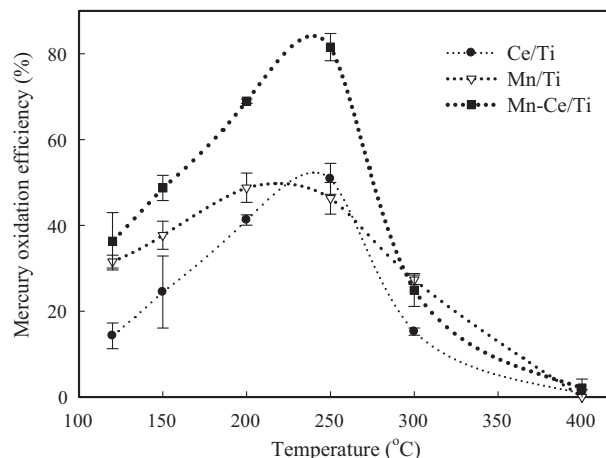


Fig. 5.  $\text{Hg}^0$  oxidation over different catalysts under simulated flue gas. The gas hourly space velocity (GHSV) was about  $120,000 \text{ h}^{-1}$ , and the simulated flue gas components were 4%  $\text{O}_2$ , 8%  $\text{H}_2\text{O}$ , 12%  $\text{CO}_2$ , 10 ppm HCl, 300 ppm NO, 400 ppm  $\text{SO}_2$  and about  $75 \mu\text{g m}^{-3} \text{Hg}^0$ .

The XPS spectra of Mn 2p, Ce 3d, Ti 2p and O 1s for different catalysts were fitted by Gaussian model, and the surface atomic concentrations of the four elements in these catalysts were calculated accordingly. As shown in Table 1, the total oxygen concentration on the Mn-Ce/Ti catalyst surface was higher than that of Mn/Ti and Ce/Ti catalysts. The higher surface oxygen concentration on the Mn-Ce/Ti catalyst was attributed to the  $\text{Mn}^{4+}$  related lattice oxygen and  $\text{Ce}^{3+}$  related chemisorbed and/or weakly bonded oxygen. In contrast, the titanium concentration on the Mn-Ce/Ti catalyst surface was lower than that of Mn/Ti and Ce/Ti catalysts. It should be noted that surface oxygen, especially the surface chemisorbed oxygen, is highly active for oxidation processes [32,46], while titanium was demonstrated to be essentially inactive for  $\text{Hg}^0$  oxidation [48]. The surface concentration of manganese on Mn-Ce/Ti was higher than that of Mn/Ti although their bulk manganese contents were the same, implying that introduction of  $\text{CeO}_2$  facilitated the dispersion of  $\text{MnO}_x$  on the catalyst surface. This is in line with the XRD results stated above.

### 3.2. Performance of different catalysts under simulated flue gas

$\text{Hg}^0$  oxidation efficiencies over Mn/Ti, Ce/Ti and Mn-Ce/Ti catalysts under simulated flue gas (SFG: 4%  $\text{O}_2$ , 8%  $\text{H}_2\text{O}$ , 12%  $\text{CO}_2$ , 10 ppm HCl, 300 ppm NO, 400 ppm  $\text{SO}_2$  and  $\sim 75 \mu\text{g m}^{-3} \text{Hg}^0$ ) are shown in Fig. 5. At low temperatures (120–200 °C),  $E_{\text{oxi}}$  over Mn/Ti catalyst was higher than that over Ce/Ti catalyst. This is in accordance with other studies [23,24,49] that manganese oxides were active for  $\text{Hg}^0$  oxidation at low temperatures. At almost the entire temperature range,  $E_{\text{oxi}}$  over Mn-Ce/Ti catalyst was higher than that over Mn/Ti and Ce/Ti catalysts. This result demonstrates the synergy for  $\text{Hg}^0$  oxidation when manganese oxides and cerium oxides are combined. This is similar to another literature [30] where Mn-Ce/Ti catalyst was more effective than Mn/Ti catalyst for selective catalytic reduction of  $\text{NO}_x$  by  $\text{NH}_3$ . Moreover, this is in accordance with the XRD and XPS results that the combination resulted in well dispersed active species and more surface oxygen, which are responsible for  $\text{Hg}^0$  oxidation.

On the Mn-Ce/Ti catalyst,  $E_{\text{oxi}}$  increased with temperature from 120 to 250 °C, and then decreased dramatically when temperature further increased from 250 to 300 °C. This is similar to that observed for the Ce/Ti catalyst, on which  $\text{Hg}^0$  oxidation was proposed to follow the Langmuir–Hinshelwood mechanism [33]. In line with the dramatic decrease of  $\text{Hg}^0$  oxidation activities, significant desorption of  $\text{Hg}^0$  with temperature increase from 250 to 300 °C was

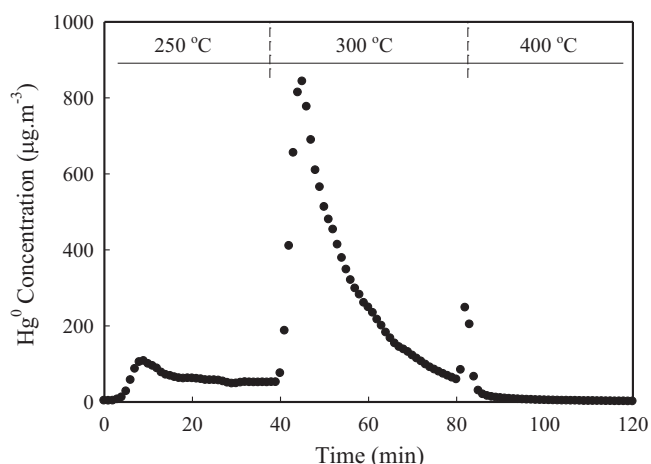


**Fig. 6.** Desorption of  $\text{Hg}^0$  by increase of temperature. 0.5 g Mn-Ce/Ti was first pre-treated at 200 °C under a flow of  $75 \mu\text{g m}^{-3}$   $\text{Hg}^0$  balanced in  $\text{N}_2$  for several hours.

observed in Fig. 6. Before the desorption experiment, 0.5 g Mn-Ce/Ti was first exposed to a gas flow of  $75 \mu\text{g m}^{-3}$   $\text{Hg}^0$  balanced in  $\text{N}_2$  at 200 °C for several hours. No obvious  $\text{Hg}^0$  desorption was observed after increasing temperature from 200 to 250 °C, while a huge spike of  $\text{Hg}^0$  was observed when the temperature further increased from 250 to 300 °C. Further increase of temperature from 300 to 400 °C resulted in insignificant desorption of  $\text{Hg}^0$ . This result demonstrates that, when temperature is lower than 250 °C, increase of temperature has no obvious effect on  $\text{Hg}^0$  adsorption capacity. However,  $\text{Hg}^0$  cannot be adsorbed efficiently on the Mn-Ce/Ti catalyst over 300 °C.

### 3.3. Performance of Mn-Ce/Ti under different flue gas conditions

As a potential low temperature SCR catalyst, Mn-Ce/Ti catalyst would probably be used under SCR conditions where  $\text{NH}_3$  is usually present [31]. Therefore, it is necessary to investigate  $\text{Hg}^0$  catalytic oxidation activity under SCR atmosphere, which in this study was defined as SFG plus  $\text{NH}_3$ , with the  $\text{NO}/\text{NH}_3$  ratio of 1. As shown in Fig. 7,  $E_{\text{oxi}}$  at 200 °C under pure  $\text{N}_2$  gas flow was observed to be around 70%, which is much larger than the  $E_{\text{oxi}}$  observed over  $\text{V}_2\text{O}_5\text{-SiO}_2$  catalyst under similar conditions [36]. Most of the  $\text{Hg}^0$  loss on the Mn-Ce/Ti under pure  $\text{N}_2$  atmosphere was due to the reaction between gas-phase or adsorbed  $\text{Hg}^0$  with stored oxygen (including lattice oxygen and chemisorbed oxygen). The large oxygen storage capacity and its low temperature activity were responsible for

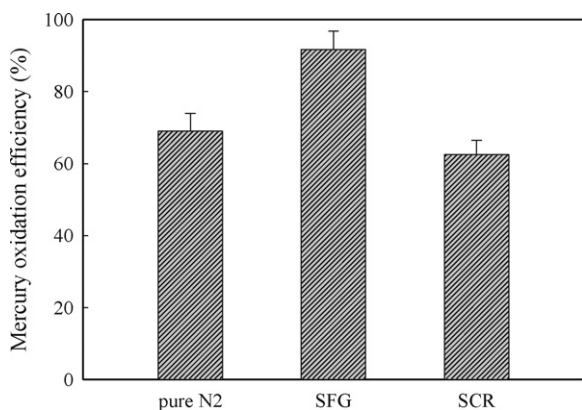


**Fig. 7.**  $\text{Hg}^0$  oxidation under different atmospheres at 200 °C. The GHSV was about  $60,000 \text{ h}^{-1}$  and feed  $\text{Hg}^0$  concentration was about  $75 \mu\text{g m}^{-3}$ ; SFG atmosphere: 4%  $\text{O}_2$ , 8%  $\text{H}_2\text{O}$ , 12%  $\text{CO}_2$ , 10 ppm HCl, 300 ppm NO and 400 ppm  $\text{SO}_2$ ; SCR atmosphere: SFG plus 300 ppm  $\text{NH}_3$ .

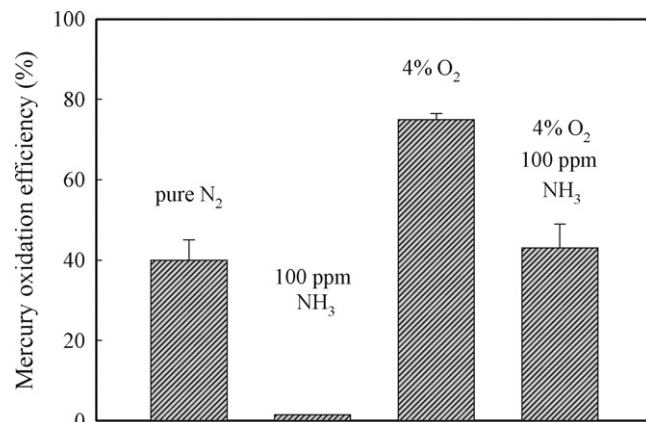


**Fig. 8.** Effect of  $\text{NH}_3$  on  $\text{Hg}^0$  oxidation at 200 °C. The GHSV was about  $120,000 \text{ h}^{-1}$  and feed  $\text{Hg}^0$  concentration was about  $75 \mu\text{g m}^{-3}$ .

this superior activity under pure  $\text{N}_2$  atmosphere. For the SFG atmosphere,  $E_{\text{oxi}}$  was higher than 90%, indicating flue gas components such as HCl, NO reacted with  $\text{Hg}^0$  with the aid of Mn-Ce/Ti catalyst. When 300 ppm  $\text{NH}_3$  was introduced into the SFG to make SCR atmosphere,  $E_{\text{oxi}}$  decreased from 91.7% to 62.5%, indicating the presence of  $\text{NH}_3$  inhibited  $\text{Hg}^0$  oxidation over the Mn-Ce/Ti catalyst. However, the  $E_{\text{oxi}}$  of 62.5% is still encouraging, since lower space velocity and higher HCl concentration of the typical flue gas would result in higher  $\text{Hg}^0$  oxidation efficiency. Furthermore, it should be noted that the inhibitive effect of  $\text{NH}_3$  on  $\text{Hg}^0$  oxidation would be insignificant in the tail-end of the actual SCR reactors, where the  $\text{NH}_3$  concentration is limited.

### 3.4. Effect of $\text{NH}_3$ on $\text{Hg}^0$ oxidation

To study the possible mechanisms involved in the deactivation of  $\text{Hg}^0$  oxidation by  $\text{NH}_3$ , 100 ppm  $\text{NH}_3$  was added to pure  $\text{N}_2$  atmosphere and gas flow containing 4%  $\text{O}_2$  balanced in  $\text{N}_2$ . As shown in Fig. 8, the addition of 100 ppm  $\text{NH}_3$  into pure  $\text{N}_2$  resulted in a significant decrease of  $E_{\text{oxi}}$  from 40.0% to 1.5%. This implies that (a)  $\text{NH}_3$  consumed the surface oxygen [28,50] which is responsible for  $\text{Hg}^0$  oxidation in pure  $\text{N}_2$  atmosphere, or (b)  $\text{NH}_3$  inhibited  $\text{Hg}^0$  adsorption [35,51] which is crucial for  $\text{Hg}^0$  oxidation through the Langmuir–Hinshelwood mechanism. When 4%  $\text{O}_2$  was present,  $E_{\text{oxi}}$  of 75.0% was higher than that (40.0%) in the pure  $\text{N}_2$  atmosphere. Gas-phase  $\text{O}_2$  regenerated the lattice oxygen and replenished the chemisorbed oxygen, which served as the  $\text{Hg}^0$  oxidant. Hence,  $E_{\text{oxi}}$  increased when  $\text{O}_2$  was introduced to the pure  $\text{N}_2$  carrier gas. The addition of  $\text{NH}_3$  also deactivated  $\text{Hg}^0$  oxidation even in the presence of  $\text{O}_2$ , with the  $E_{\text{oxi}}$  decreased from 75.0% to 43.0%, which, however, was much higher than the  $E_{\text{oxi}}$  under 100 ppm  $\text{NH}_3$  without  $\text{O}_2$ . This indicates that the presence of gas-phase  $\text{O}_2$  offsets part of the inhibitive effect of  $\text{NH}_3$ . Therefore, it can be concluded that consumption of surface oxygen by  $\text{NH}_3$  was at least partly responsible for the deactivation of  $\text{Hg}^0$  oxidation. Besides this reason, inhibition of  $\text{Hg}^0$  adsorption by  $\text{NH}_3$  has also been demonstrated over the Mn-Ce/Ti catalyst. As shown in Fig. 9, a significant increase of  $\text{Hg}^0$  concentration was observed after cutting off  $\text{Hg}^0$  and adding 100 ppm  $\text{NH}_3$  at the same time. Without adding  $\text{NH}_3$ , in contrast,  $\text{Hg}^0$  concentration decreased gradually after stopping  $\text{Hg}^0$ . The result demonstrates that both  $\text{Hg}^0$  and  $\text{NH}_3$  competed for the active sites, and the affinity between  $\text{NH}_3$  and Mn-Ce/Ti catalyst was stronger than that between  $\text{Hg}^0$  and Mn-Ce/Ti catalyst. Further studies are needed to identify whether reactions between  $\text{NH}_3$  and other flue gas components inhibit  $\text{Hg}^0$  oxidation or not, even though the reactions between  $\text{SO}_2$  and  $\text{NH}_3$  over Mn/Ti catalyst were found to be greatly inhibited by doping of  $\text{CeO}_2$  [42].

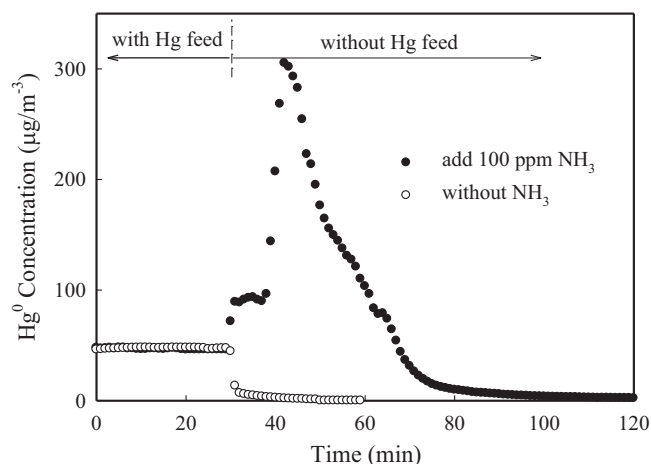


**Fig. 9.** Desorption of  $\text{Hg}^0$  by  $\text{NH}_3$  at  $200^\circ\text{C}$ .  $0.5\text{ g}$  Mn-Ce/Ti was first pretreated at  $200^\circ\text{C}$  under a flow of  $75\text{ }\mu\text{g m}^{-3}$   $\text{Hg}^0$  balanced in  $\text{N}_2$  for several hours.

### 3.5. Recovery of catalyst after cutting off $\text{NH}_3$

Even though  $\text{NH}_3$  inhibited  $\text{Hg}^0$  oxidation over Mn-Ce/Ti catalyst by consuming surface oxygen and limiting  $\text{Hg}^0$  adsorption, recovery of  $\text{Hg}^0$  oxidation activity over Mn-Ce/Ti catalyst can be achieved quickly after cutting off  $\text{NH}_3$ , especially in the presence of  $\text{O}_2$ . As shown in Fig. 10(a), in the presence of 4%  $\text{O}_2$ , about 0.25 of feed  $\text{Hg}^0$  was detected downstream the catalyst, while about 0.6 of feed  $\text{Hg}^0$  was detected after the catalyst with the gas flow containing

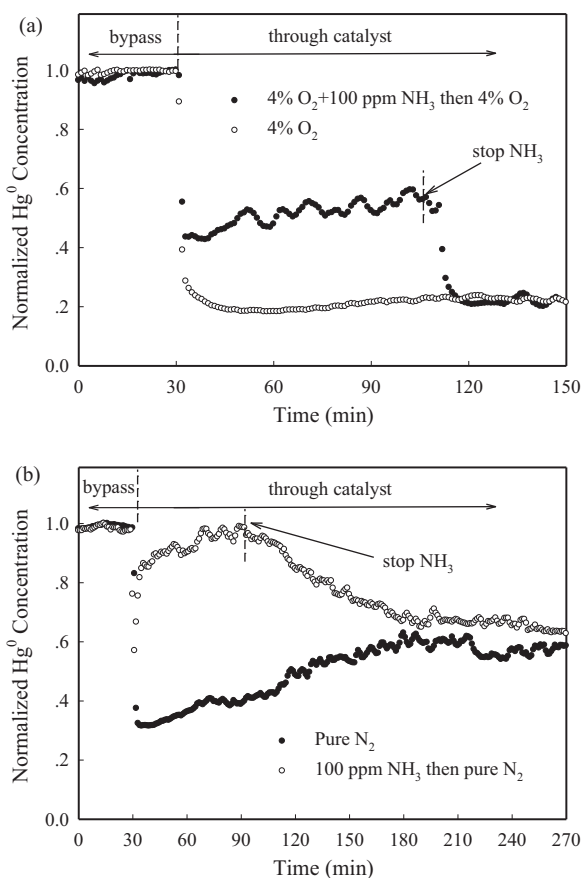


**Fig. 10.** Catalyst recovery after cutting off  $\text{NH}_3$  at  $200^\circ\text{C}$ : (a) in the presence of  $\text{O}_2$ ; (b) in the absence of  $\text{O}_2$ . The GHSV was about  $120,000\text{ h}^{-1}$  and feed  $\text{Hg}^0$  concentration was about  $75\text{ }\mu\text{g m}^{-3}$ .

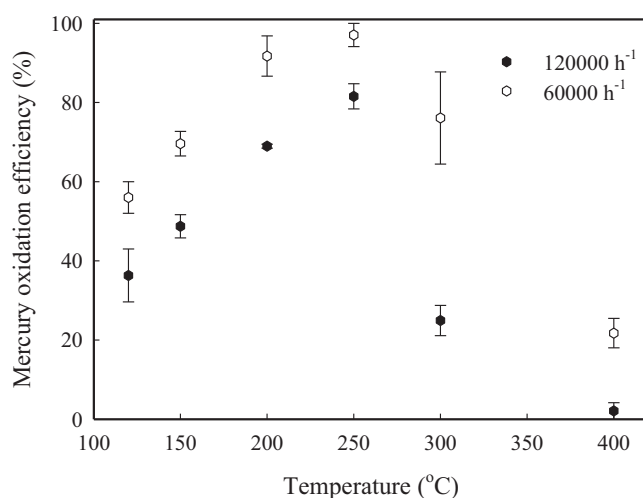


**Fig. 11.** Effect of GHSV on  $\text{Hg}^0$  oxidation under simulated flue gas condition. Flue gas components were 4%  $\text{O}_2$ , 8%  $\text{H}_2\text{O}$ , 12%  $\text{CO}_2$ , 10 ppm HCl, 300 ppm NO, 400 ppm  $\text{SO}_2$  and about  $75\text{ }\mu\text{g m}^{-3}$   $\text{Hg}^0$ .

4%  $\text{O}_2$  plus 100 ppm  $\text{NH}_3$ . After stopping  $\text{NH}_3$  at 105 min, the outlet  $\text{Hg}^0$  concentration quickly (in less than 15 min) decreased to the same level as that observed under the flue gas without  $\text{NH}_3$ . With this merit of the Mn-Ce/Ti catalyst, high  $\text{Hg}^0$  oxidation efficiency can be easily achieved once  $\text{NH}_3$  was consumed in the SCR reactions, since higher than 90%  $\text{Hg}^0$  oxidation was observed under such adverse conditions stated in Section 3.3. As shown in Fig. 10(b), in the absence of  $\text{O}_2$ , most of the  $\text{Hg}^0$  oxidation activity can also be achieved by stopping  $\text{NH}_3$ . However, compared to the scenario with  $\text{O}_2$ , a longer time was needed for the recovery and complete recovery was not obtained during our experimental period. This again implies that consumption of surface oxygen by  $\text{NH}_3$  was partly responsible for the deactivation of  $\text{Hg}^0$  oxidation, but its contribution was minor compared to the contribution of inhibition of  $\text{Hg}^0$  adsorption.

### 3.6. Effect of gas hourly space velocity

Gas hourly space velocity (GHSV) is a crucial parameter for the practical application. To achieve high  $\text{Hg}^0$  oxidation efficiency, high  $\text{Hg}^0$  oxidation activity at high space velocity is required for catalysts. This is important especially for those used for selective catalytic reductive of  $\text{NO}_x$  with  $\text{NH}_3$ , because of the small volume of the  $\text{NH}_3$ -free or  $\text{NH}_3$ -deficient space at the tail-end of the actual SCR reactor, where  $\text{Hg}^0$  oxidation efficiency is relatively higher. The activities of the Mn-Ce/Ti catalyst at high GHSV of 60,000 and  $120,000\text{ h}^{-1}$  were studied under simulated low-rank coal combustion flue gas atmosphere. As shown in Fig. 11, in the entire temperature range,  $E_{\text{oxi}}$  decreased as GHSV increased from 60,000 to  $120,000\text{ h}^{-1}$ . However, the huge increase of GHSV from 60,000 to  $120,000\text{ h}^{-1}$  only resulted in about 10% decrease of  $E_{\text{oxi}}$  when temperature was below  $250^\circ\text{C}$ . The  $E_{\text{oxi}}$  at a GHSV of  $120,000\text{ h}^{-1}$ , which is about 50 times higher than the GHSV in actual SCR reactors, can still reach 80% at the optimal operating temperatures.

## 4. Discussions

In this study, the composition of the simulated flue gas was in the range of those flue gases from burning low-rank coals, and the GHSV of  $60,000$  or  $120,000\text{ h}^{-1}$  was much higher than the typical GHSV ( $2000$ – $4000\text{ h}^{-1}$ ) in power plant SCR reactors [52]. Under these adverse conditions, the  $E_{\text{oxi}}$  over Mn-Ce/Ti at the optimal operating temperatures was still higher than 90% (Fig. 7). The presence

of  $\text{NH}_3$  in the simulated flue gas inhibited  $\text{Hg}^0$  oxidation over Mn-Ce/Ti catalyst. However, once  $\text{NH}_3$  was cut off the inhibited  $\text{Hg}^0$  oxidation activity could be completely recovered in the presence of  $\text{O}_2$ . This indicates that at the tail-end of the SCR reactor, where the  $\text{NH}_3$  concentration is limited, the  $E_{\text{oxi}}$  would be as high as that for SFG. Although the  $\text{NH}_3$ -free or  $\text{NH}_3$ -deficient space at the tail-end of the actual SCR reactor is small, the high  $\text{Hg}^0$  oxidation activity of Mn-Ce/Ti catalyst at high GHSV could warrant a high  $\text{Hg}^0$  oxidation efficiency, i.e. more than 60%  $\text{Hg}^0$  was observed to be oxidized on the Mn-Ce/Ti catalyst at 200 °C under simulated SCR flue gas with low HCl concentration and extremely high GHSV. Moreover, optimization of the Mn-Ce/Ti content in the future would probably yield an even better  $\text{Hg}^0$  oxidation performance. Therefore, the applications of the Mn-Ce/Ti catalyst either as an exclusive  $\text{Hg}^0$  oxidation catalyst or as a low temperature SCR catalyst very likely are beneficial to  $\text{Hg}^0$  oxidation for coal-fired power plants because both higher HCl concentration in high-rank coal combustion flue gases and lower space velocity have been reported to facilitate  $\text{Hg}^0$  conversion [13,53]. In addition, high activities of Mn-Ce/Ti catalysts at low temperatures allow them to be placed downstream of PM control devices, where deactivation by exposure to high concentration of fly ash is minimized [22,24].

Deacon process, the Eley–Rideal mechanism and the Langmuir–Hinshelwood mechanism have been proposed for heterogeneous mercury oxidation in the presence of HCl [11]. Because of the low HCl to  $\text{Cl}_2$  conversion rate [11] and low reaction rate between gas-phase  $\text{Cl}_2$  and  $\text{Hg}^0$  at this temperature range [53], Deacon process is not enough to account for the observed extent of mercury oxidation. Generally, higher temperature accelerates chemical reactions. Hence, if active species over Mn-Ce/Ti catalyst can react with gas-phase  $\text{Hg}^0$  through the Eley–Rideal mechanism,  $\text{Hg}^0$  oxidation efficiency should increase with temperature increase. However,  $\text{Hg}^0$  oxidation efficiency decreased with temperature increase from 250 to 400 °C. Therefore, it is very likely that  $\text{Hg}^0$  oxidation over Mn-Ce/Ti catalyst follows the Langmuir–Hinshelwood mechanism, where reactive species on catalyst surface react with adjacently weakly adsorbed  $\text{Hg}^0$  to form  $\text{Hg}^{2+}$  [51,54]. If the increase of temperature limits the adsorption of  $\text{Hg}^0$ , it can greatly inhibit the subsequent  $\text{Hg}^0$  oxidation through the Langmuir–Hinshelwood mechanism. As demonstrated in Fig. 6, when temperature was lower than 250 °C, increase of temperature had no obvious effect on  $\text{Hg}^0$  adsorption capacity. Therefore, as shown in Fig. 5,  $\text{Hg}^0$  oxidation efficiency increased as temperature increased from 120 to 250 °C because the catalyst was more active at higher temperatures. In contrast, when temperature was higher than 300 °C, only negligible  $\text{Hg}^0$  could be adsorbed on the Mn-Ce/Ti catalyst. It is hard for  $\text{Hg}^0$  oxidation through the Langmuir–Hinshelwood mechanism to occur without enough adsorbed  $\text{Hg}^0$ . Accordingly,  $\text{Hg}^0$  oxidation efficiency was low at high temperatures.

## 5. Conclusions

Significant synergy was achieved for  $\text{Hg}^0$  oxidation when  $\text{MnO}_x$  and  $\text{CeO}_2$  were combined. The Mn-Ce/Ti catalyst was highly active for  $\text{Hg}^0$  oxidation at low flue gas temperatures under either SFG or SCR conditions. Over 90% of  $\text{Hg}^0$  oxidation was obtained on the Mn-Ce/Ti catalyst at 200–250 °C under simulated flue gas representing those from burning low-rank coals with a GHSV of 60,000  $\text{h}^{-1}$  which is more than 10 times higher than the actual GHSV in SCR reactors. A likely reaction pathway for  $\text{Hg}^0$  oxidation on the Mn-Ce/Ti catalyst is the Langmuir–Hinshelwood mechanism, where reactive species on catalyst surface react with adjacently adsorbed  $\text{Hg}^0$  to form  $\text{Hg}^{2+}$ .  $\text{NH}_3$  consumed surface oxygen and limited  $\text{Hg}^0$  adsorption; hence, it could inhibit  $\text{Hg}^0$  oxidation over the Mn-Ce/Ti

catalyst. However, once  $\text{NH}_3$  was cut off, the inhibited mercury oxidation activity could be completely recovered in the presence of  $\text{O}_2$ .

This study revealed the possibility of oxidizing  $\text{Hg}^0$  over a potential low-temperature SCR catalyst. Such knowledge is of fundamental importance in developing effective pollution control technologies and devices in which simultaneous  $\text{NO}_x$  removal and  $\text{Hg}^0$  oxidation at low temperature are possible. Future work should investigate the kinetic rate to quantitatively confirm the proposed mechanism, and optimize the catalyst composition to study  $\text{NO}_x$  removal and  $\text{Hg}^0$  oxidation simultaneously.

## Acknowledgments

This project was partially supported by the National Key Basic Research and Development Program (973) (No. 2010CB227003) and the China Scholarship Council (CSC). We thank VICI Metronics, Inc. for supplying the  $\text{Hg}$  permeation device.

## References

- [1] J.H. Pavlish, E.A. Sondreal, M.D. Mann, E.S. Olson, K.C. Galbreath, D.L. Laudal, S.A. Benson, *Fuel Process. Technol.* 82 (2003) 89–165.
- [2] U.S. EPA, Office of Air Quality Planning and Standards and Office of Research and Development, Mercury Study Report to Congress Volume I: Executive Summary, Report number: EPA-452/R-97-003, Washington, DC, December, 1997.
- [3] E.J. Granite, H.W. Pennline, R.A. Hargis, *Ind. Eng. Chem. Res.* 39 (2000) 1020–1029.
- [4] J.B. Milford, A. Pienciak, *Environ. Sci. Technol.* 43 (2009) 2669–2673.
- [5] U.S. EPA, <http://www.epa.gov/airquality/powerplanttoxics/actions.html> (accessed on 10.07.2011).
- [6] Y. Zhuang, J.S. Thompson, C.J. Zygarlicke, J.H. Pavlish, *Environ. Sci. Technol.* 38 (2004) 5803–5808.
- [7] C.L. Senior, J.J. Helble, A.F. Sarofim, *Fuel Process. Technol.* 65 (2000) 263–288.
- [8] K.C. Galbreath, C.J. Zygarlicke, *Environ. Sci. Technol.* 30 (1996) 2421–2426.
- [9] S.X. Wang, L. Zhang, G.H. Li, Y. Wu, J.M. Hao, N. Pirrone, F. Sprovieri, M.P. Ancora, *Atmos. Chem. Phys.* 10 (2010) 1183–1192.
- [10] K.C. Galbreath, C.J. Zygarlicke, J.E. Tibbetts, R.L. Schulz, G.E. Dunham, *Fuel Process. Technol.* 86 (2005) 429–448.
- [11] A.A. Presto, E.J. Granite, *Environ. Sci. Technol.* 40 (2006) 5601–5609.
- [12] C. Senior, Oxidation of Mercury Across SCR Catalysts in Coal-Fired Power Plants Burning Low Rank Fuels, DOE Quarterly Progress Report (DE-FC26-03NT41728), 2004.
- [13] C.L. Senior, *J. Air Waste Manage. Assoc.* 56 (2006) 23–31.
- [14] H.M. Yang, W.P. Pan, *J. Environ. Sci. (China)* 19 (2007) 181–184.
- [15] D. Pudasainee, S.J. Lee, S.H. Lee, J.H. Kim, H.N. Jang, S.J. Cho, Y.C. Seo, *Fuel* 89 (2010) 804–809.
- [16] S.A. Benson, J.D. Laumb, C.R. Crocker, J.H. Pavlish, *Fuel Process. Technol.* 86 (2005) 577–613.
- [17] T.J. Feeley, L.A. Brickett, J.T. Murphy, Evaluation of the Effect of SCR  $\text{NO}_x$  Control Technology on Mercury Speciation, Report of U.S. DOE, 2003.
- [18] P.R. Ettireddy, N. Ettireddy, S. Mamedov, P. Boolchand, P.G. Smirniotis, *Appl. Catal. B* 76 (2007) 123–134.
- [19] P.G. Smirniotis, D.A. Peña, B.S. Uphade, *Angew. Chem. Int. Ed.* 40 (2001) 2479–2482.
- [20] D.A. Peña, B.S. Uphade, P.G. Smirniotis, *J. Catal.* 221 (2004) 421–431.
- [21] Y.J. Kim, H.J. Kwon, I.S. Nam, J.W. Choung, J.K. Kil, H.J. Kim, M.S. Cha, G.K. Yeo, *Catal. Today* 151 (2010) 244–250.
- [22] Z. Wu, B. Jiang, Y. Liu, W. Zhao, B. Guan, *J. Hazard. Mater.* 145 (2007) 488–494.
- [23] L. Ji, P.M. Sreekanth, P.G. Smirniotis, S.W. Thiel, N.G. Pinto, *Energy Fuels* 22 (2008) 2299–2306.
- [24] J.F. Li, N.Q. Yan, Z. Qu, S.H. Qiao, S.J. Yang, Y.F. Guo, P. Liu, J.P. Jia, *Environ. Sci. Technol.* 44 (2010) 426–431.
- [25] S. Qiao, J. Chen, J. Li, Z. Qu, P. Liu, N. Yan, J. Jia, *Ind. Eng. Chem. Res.* 48 (2009) 3317–3322.
- [26] B.M. Reddy, A. Khan, Y. Yamada, T. Kobayashi, S. Loidant, J.C. Volta, *J. Phys. Chem. B* 107 (2003) 5162–5167.
- [27] G.S. Qi, R.T. Yang, *J. Phys. Chem. B* 108 (2004) 15738–15747.
- [28] G.S. Qi, R.T. Yang, R. Chang, *Appl. Catal. B* 51 (2004) 93–106.
- [29] G.S. Qi, R.T. Yang, *J. Catal.* 217 (2003) 434–441.
- [30] Z. Wu, R. Jin, Y. Liu, H. Wang, *Catal. Commun.* 9 (2008) 2217–2220.
- [31] R. Jin, Y. Liu, Z. Wu, H. Wang, T. Gu, *Chemosphere* 78 (2010) 1160–1166.
- [32] L. Chen, J. Li, M. Ge, R. Zhu, *Catal. Today* 153 (2010) 77–83.
- [33] H. Li, C.Y. Wu, Y. Li, J. Zhang, *Environ. Sci. Technol.* 45 (2011) 7394–7400.
- [34] H. Li, Y. Li, C.Y. Wu, J. Zhang, *Chem. Eng. J.* 169 (2011) 186–193.
- [35] S. Eswaran, H.G. Stenger, *Energy Fuels* 19 (2005) 2328–2334.
- [36] Y. Li, P.D. Murphy, C.Y. Wu, K.W. Powers, J.C.J. Bonzongo, *Environ. Sci. Technol.* 42 (2008) 5304–5309.
- [37] Y. Cao, B. Chen, J. Wu, H. Cui, J. Smith, C.K. Chen, P. Chu, W.P. Pan, *Energy Fuel* 21 (2007) 145–156.

- [38] H. Kamata, S.I. Ueno, T. Naito, A. Yukimura, *Ind. Eng. Chem. Res.* 47 (2008) 8136–8141.
- [39] W. Xu, Y. Yu, C. Zhang, H. He, *Catal. Commun.* 9 (2008) 1453–1457.
- [40] M. Luo, J. Chen, L. Chen, J. Lu, Z. Feng, C. Li, *Chem. Mater.* 13 (2000) 197–202.
- [41] J. Villaseñor, P. Reyes, G. Pecchi, *Catal. Today* 76 (2002) 121–131.
- [42] Z. Wu, R. Jin, H. Wang, Y. Liu, *Catal. Commun.* 10 (2009) 935–939.
- [43] M. Kang, E.D. Park, J.M. Kim, J.E. Yie, *Appl. Catal. A* 327 (2007) 261–269.
- [44] P. Burroughs, A. Hammet, A.F. Orchard, G. Thornton, *J. Chem. Soc. Dalton Trans.* 168 (1976) 6–1698.
- [45] D.R. Mullins, S.H. Overbury, D.R. Huntley, *Surf. Sci.* 409 (1998) 307–319.
- [46] S. Yang, W. Zhu, Z. Jiang, Z. Chen, J. Wang, *Appl. Surf. Sci.* 252 (2006) 8499–8505.
- [47] L. Chen, J.H. Li, M.F. Ge, *J. Phys. Chem. C* 113 (2009) 21177–21184.
- [48] H. Kamata, S.I. Ueno, T. Naito, A. Yamaguchi, S. Ito, *Catal. Commun.* 9 (2008) 2441–2444.
- [49] Y. Wang, Y. Duan, *Energy Fuels* 25 (2011) 1553–1558.
- [50] Z.Y. Ding, L. Li, D. Wade, E.F. Gloyne, *Ind. Eng. Chem. Res.* 37 (1998) 1707–1716.
- [51] Y. Eom, S.H. Jeon, T.A. Ngo, J. Kim, T.G. Lee, *Catal. Lett.* 121 (2008) 219–225.
- [52] D.L. Laudal, J.S. Thompson, J.H. Pavlish, L. Brickett, P. Chu, R.K. Srivastava, C.W. Lee, J.D. Kilgroe, 3rd International Air Quality Conference, Arlington, Virginia, September, 2002.
- [53] S. Niksa, N. Fujiwara, *J. Air Waste Manage. Assoc.* 55 (2005) 1866–1875.
- [54] S. He, J. Zhou, Y. Zhu, Z. Luo, M. Ni, K. Cen, *Energy Fuels* 23 (2009) 253–259.